Anderson Delocalization in Strongly Coupled Disordered Non-Hermitian Chains

Wei-Wu Jin,[1,*] Jin Liu,[1,*] Xin Wang,[2] Yu-Ran Zhang,[1] Xueqin Huang,[1] Xiaomin Wei,[1] Wenbo Ju,[1,†] Zhongmin Yang,[1,3,4,‡] Tao Liu,[1,§] and Franco Nori[5,6]

[1]*School of Physics and Optoelectronics, South China University of Technology, Guangzhou 510640, China*
[2]*Institute of Theoretical Physics, School of Physics, Xi'an Jiaotong University, Xi'an 710049, China*
[3]*Research Institute of Future Technology, South China Normal University, Guangzhou 510006, China*
[4]*State Key Laboratory of Luminescent Materials and Devices and Institute of Optical Communication Materials, South China University of Technology, Guangzhou 510640, China*
[5]*Center for Quantum Computing, RIKEN, Wakoshi, Saitama 351-0198, Japan*
[6]*Department of Physics, University of Michigan, Ann Arbor, Michigan 48109-1040, USA*

(Received 22 December 2024; revised 3 May 2025; accepted 24 July 2025; published 12 August 2025)

Disorder and non-Hermitian effects together can upend how waves localize. In a 1D disordered chain, the non-Hermitian skin effect (NHSE) can induce Anderson delocalization, defying the usual rule that disorder in low dimensions always localizes states. While weak disorder leaves the NHSE intact, strong disorder restores Anderson localization. Here, we study a surprising twist: coupling a strongly disordered Hatano-Nelson chain to a disordered Hermitian chain with their disorder antisymmetrically correlated. Strikingly, once the interchain coupling exceeds a threshold, the system undergoes Anderson delocalization irrespective of disorder strength, reinstating the NHSE with no Hermitian counterpart. This transition arises from the interplay of nonreciprocal hopping, interchain coupling, and engineered disorder correlations, and is captured by a real-space winding number. To confirm this, we build an electrical-circuit analog and directly observe the reemergent NHSE via voltage measurements. Our Letter uncovers unexplored and experimentally accessible physics at the crossroads of non-Hermiticity and disorder.

DOI: 10.1103/lpm2-vcb4

Introduction—Recent years have seen growing interest in exotic physics emerging from non-Hermitian systems [1–24]. These include platforms such as optical setups [25–33], electrical circuits [34–39], and open quantum systems [40,41]. A central discovery is the non-Hermitian skin effect (NHSE) [3–6], where bulk modes become highly sensitive to boundaries and localize at the edges under open boundary conditions. This effect, rooted in point-gap topology [6,7], drives many novel phenomena without Hermitian analogs, such as the breakdown of conventional Bloch band theory [3] and disorder-free entanglement phase transitions [21].

Disorder plays a crucial role in non-Hermitian systems, impacting transport, entanglement, and topology [42–56]. It induces exotic phenomena such as nonunitary scaling in localization [46], disorder-induced non-Bloch topological phase transitions [55], and coexistence of dynamical delocalization and spectral localization [54]. A seminal study by Hatano and Nelson extended the one-dimensional (1D) Anderson model by introducing nonreciprocal hopping [42], revealing unexpected delocalization with the emergence of NHSE under weak disorder. This challenges the conventional expectation that disordered systems in less than two dimensions are always localized [57]. Their findings showed that non-Hermiticity can fundamentally alter Anderson localization in the 1D Hatano-Nelson (HN) chain. However, as disorder strength increases, the skin modes eventually localize again, highlighting a complex interplay between disorder and non-Hermiticity. This reentrant behavior raises a compelling question: can a strongly disordered non-Hermitian system exhibit an Anderson localization-delocalization transition that revives the NHSE?

In Hermitian systems, coupling between disordered chains has been shown to induce delocalization [58–64], suggesting a potential route to explore similar transitions in the non-Hermitian field. Inspired by this, we explore the Anderson localization-delocalization behavior of coupled non-Hermitian chains in a ladder geometry subjected to ultrastrong disorder. Our Letter aims to uncover novel mechanisms driving Anderson localization-delocalization transitions that revive the NHSE, offering deeper insights into the intricate interplay among non-Hermiticity, disorder, and interchain coupling in extended systems.

In this Letter, we uncover a novel topological Anderson localization-delocalization transition in coupled disordered chains, driven by the interplay of non-Hermiticity, interchain coupling, and correlated disorder. Our hybrid system

*These authors contributed equally to this work.
†Contact author: wjuphy@scut.edu.cn
‡Contact author: yangzm@scut.edu.cn
§Contact author: liutao0716@scut.edu.cn

consists of a non-Hermitian HN chain coupled to a Hermitian chain with antisymmetrically correlated disorder. Remarkably, this configuration leads to an Anderson delocalization transition that revives the NHSE even under ultrastrong disorder, with the interchain coupling strength controlling the reemergence of the NHSE. This transition is topologically characterized by the real-space winding number. Experimental realization using tunable nonreciprocal electrical circuits confirms these findings, highlighting how non-Hermiticity and correlated disorder together govern wave localization.

Model—We start by considering an HN chain with asymmetric hopping [42], which shows the NHSE. Adding random on-site disorder leads to Anderson delocalization at weak disorder [42–46]. As the disorder strength increases further, Anderson localization eventually takes over. In this Letter, we demonstrate that Anderson delocalization, accompanied by reemergent NHSE, can be restored even in the ultrastrong disorder regime by coupling the disordered HN chain to a disordered Hermitian chain with correlated disorder, as illustrated in Fig. 1(a). The Hamiltonian of the hybrid system is written as

$$\begin{aligned}\hat{\mathcal{H}} = &\sum_j [(\gamma+\lambda)\hat{a}_j^\dagger \hat{a}_{j+1} + (\gamma-\lambda)\hat{a}_{j+1}^\dagger \hat{a}_j] \\ &+ \sum_j (J\hat{b}_{j+1}^\dagger \hat{b}_j + t\hat{a}_j^\dagger \hat{b}_j + \text{H.c.}) \\ &+ \sum_j (\Delta_j^{(a)} \hat{a}_j^\dagger \hat{a}_j + \Delta_j^{(b)} \hat{b}_j^\dagger \hat{b}_j), \end{aligned} \tag{1}$$

where $\hat{a}_j^\dagger$ and $\hat{b}_j^\dagger$ are creation operators for the HN and Hermitian chains at jth unit cell, $\gamma \pm \lambda$ denote the asymmetric hopping, J is the symmetric hopping strength, t is the interchain coupling strength, and $\Delta_j^{(\mu)}$ $(\mu = a, b)$ is the random on-site potential, applied to the HN $(\mu = a)$ and Hermitian $(\mu = b)$ chains, which is uniformly sampled in $[-W/2, W/2]$, with W being the disorder strength.

Although uncorrelated strong random disorder leads to Anderson localization in both the HN chain and the coupled chains, we will show that the reemergence of the NHSE can occur if an appropriately correlated disorder is applied to the coupled chains. We consider two types of correlated disorder schemes: symmetric disorder with $\Delta_j^{(a)} = \Delta_j^{(b)} = \Delta_j$, and antisymmetric disorder with $\Delta_j^{(a)} = -\Delta_j^{(b)} = \Delta_j$.

Figures 1(b)–1(e) plot the probability density distributions $|\psi_n^{(a)}(j)|^2$ and $|\psi_n^{(b)}(j)|^2$ of right eigenstates under ultrastrong on-site disorder, and the corresponding complex eigenenergies under periodic (PBC) and open (OBC) boundary conditions. In the presence of symmetrically correlated disorder, all states in the coupled HN-Hermitian chains remain localized [see Fig. 1(b)]. The absence of point gaps in Fig. 1(d) further indicates the breakdown of the NHSE. However, when antisymmetrically correlated disorder is

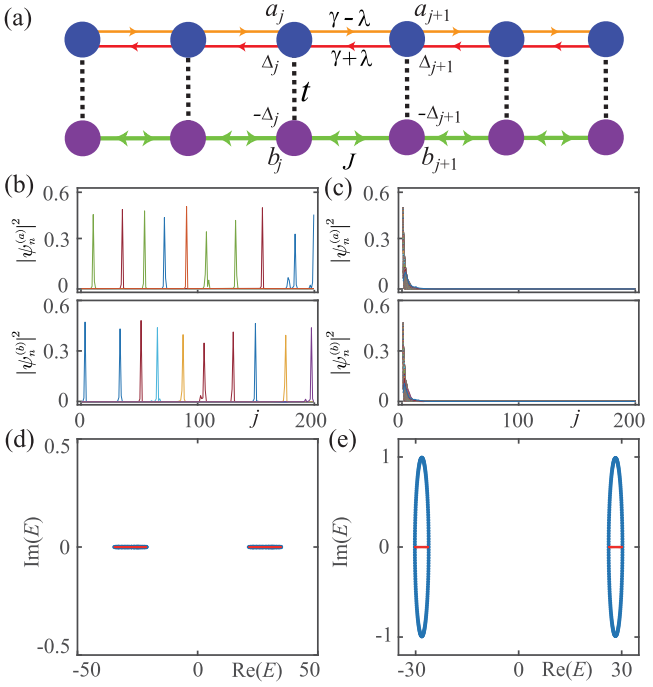

FIG. 1. (a) Schematic showing a disordered HN chain (top) coupled to a disordered Hermitian chain (bottom). $\gamma \pm \lambda$ denote the asymmetric hopping strengths, J is the symmetric hopping strength, and t is the interchain coupling strength. The antisymmetric random on-site potential Δ_j and $-\Delta_j$ are applied to each chain. (b),(c) Probability density distributions $|\psi_n^{(a)}(j)|^2$ and $|\psi_n^{(b)}(j)|^2$ of the coupled chains subject to symmetric random potential with $\Delta_j^{(a)} = \Delta_j^{(b)} = \Delta_j$ (b), and antisymmetric random potential with $\Delta_j^{(a)} = -\Delta_j^{(b)} = \Delta_j$ (c). All eigenstates exhibit Anderson localization, where only a few are plotted in (b) for clarity from one disorder realization. Plots in (d),(e) show the corresponding complex eigenenergies under PBC (blue dots) and OBC (red dots). The parameters used are $\gamma/J = \lambda/J = 1$, $W/J = 12$, $t/J = 28$, and $N = 200$.

introduced, the complex eigenspectrum under PBC (blue dots) forms two point gaps at large interchain coupling strength t [see Fig. 1(e)], which encircle the eigenenergies under OBC (red dots). As shown in Fig. 1(c), all states inside the point gaps are localized at the left boundary, signaling the reemergence of the NHSE. Note that the eigenstates in the coupled Hermitian chains remain localized despite antisymmetric disorder. This highlights that the Anderson delocalization accompanied by reemergent NHSE in a disordered nonreciprocal chain, coupled to a Hermitian chain with antisymmetric disorder, is a genuinely nontrivial phenomenon without a Hermitian counterpart.

The hidden physical mechanism can be intuitively understood by considering the strong interchain coupling case with $|t \gg |J, |\gamma \pm \lambda|, |\Delta_j|$ for both symmetric and antisymmetric disorder configurations (see Sec. I of Supplemental Material (SM) [65]). In this limit, rewriting $\hat{\mathcal{H}}$ in the new

basis $|\alpha_{\pm}, j\rangle = \hat{\alpha}^{\dagger}_{\pm,j}|0\rangle$, with $\hat{\alpha}_{\pm,j} = (\pm\hat{a}_j + \hat{b}_j)/\sqrt{2}$, yields an effective nonreciprocal Creutz ladder subject to on-site random potentials $\Delta_j \pm t$ and $\pm\sqrt{t^2 + \Delta_j^2}$ for symmetric and antisymmetric disorder configurations, respectively. For symmetric disorder, the effective Creutz ladder undergoes Anderson localization under strong disorder Δ_j. However, for antisymmetric disorder, the effective disorder strength $\tilde{W}$ becomes $\tilde{W} < W^2/|8t|$ [65]. In the strong interchain coupling limit $|t| \gg W$, $\tilde{W}$ becomes much smaller than the nonreciprocal hopping strength λ of the Creutz ladder. While an arbitrarily small amount of disorder induces Anderson localization in 1D Hermitian systems [57] (see also Sec. IV of SM [65]), the interplay between nonreciprocal hopping and disorder can instead lead to an Anderson transition [42,45]. Consequently, increasing interchain coupling t drives the Anderson delocalization with the reemergent NHSE, even under arbitrarily strong antisymmetric disorder.

To further characterize the Anderson localization-delocalization transition induced by the antisymmetrically correlated disorder, we calculate the inverse participation ratio (IPR) of each normalized right eigenstate $\psi_n = (\psi_n^{(a)}, \psi_n^{(b)})^T$, defined as

$$\mathrm{IPR}_n = \sum_{j=1}^{N} (|\psi_n^{(a)}(j)|^4 + |\psi_n^{(b)}(j)|^4). \tag{2}$$

Here, $\mathrm{IPR}_n \simeq 1/(2N)$ for an extended eigenstate ψ_n and vanishes as $N \to \infty$, while for a state localized over $M \ll N$ sites, $\mathrm{IPR}_n \simeq 1/M$ and remains finite in the thermodynamic limit.

However, the IPR cannot distinguish skin-mode localization from Anderson localization. To resolve skin modes, we compute the mean center of mass (mcom) of the squared amplitudes of all right eigenvectors ψ_n, averaged over disorder realizations [67], defined as

$$\mathrm{mcom} = \frac{\sum_{j=1}^{N} j\langle \mathcal{A}(j)\rangle}{\sum_{j=1}^{N} \langle \mathcal{A}(j)\rangle}, \tag{3}$$

with the mean amplitude squared of all right eigenstates

$$\langle \mathcal{A}(j)\rangle = \left\langle \frac{1}{2N} \sum_{n=1}^{2N} (|\psi_n^{(a)}(j)|^2 + |\psi_n^{(b)}(j)|^2) \right\rangle, \tag{4}$$

where $\langle\cdot\rangle$ denotes averaging over disorder realizations. When mcom is close to 1 or N, it indicates that the eigenstates are localized at the boundaries, with the emergence of NHSE. As explained in Sec. II of the SM [65], the IPR and mcom averaged over all eigenmodes effectively resolve delocalized and extended states and distinguish skin-mode localization from Anderson localization. In addition, to avoid finite-size effects (see details in Sec. III of SM [65]), we perform our calculations on a large lattice.

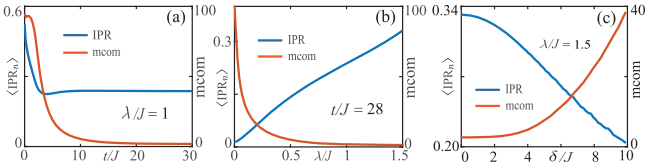

FIG. 2. (a)–(c) IPR and mcom averaged over all eigenstates, under antisymmetric disorder—(a) as a function of t with $\lambda/J = 1$, (b) as a function of λ with $t/J = 28$, and (c) as a function of δ with $\lambda/J = 1.5$, where a random perturbation $\delta_j \in [-\delta/2, \delta/2]$ breaks the exact antisymmetry. The results are averaged over 2000 disorder realizations with $\gamma/J = 1$, $W/J = 12$ and $N = 200$.

Figures 2(a) and 2(b) show the averaged IPR and mcom under antisymmetric disorder as functions of interchain coupling t and asymmetric hopping λ, respectively. Strong disorder ($W/J = 12$) induces Anderson localization at small t [Fig. 2(a)], while increasing t triggers Anderson delocalization and revives the NHSE with boundary-localized eigenstates. Furthermore, with fixed disorder ($W/J = 12$) and hopping strength ($t/J = 28$), Anderson delocalization occurs only when λ exceeds a critical value, highlighting the necessity of strong nonreciprocal hopping and interchain coupling for the reemergence of the NHSE under strong antisymmetric disorder. Note that the IPR based on biorthogonal eigenvectors shows the same localization behavior as that using right eigenvectors alone, as shown in Sec. IV of SM [65]. In addition, the reemergent NHSE can be further revealed through quenched evolution dynamics (see details in Sec. V of SM [65]).

We now investigate the robustness of this phenomenon under deviations from exact antisymmetric disorder. To this end, we consider a modified disorder configuration with $\Delta_j^{(a)} = \Delta_j$ and $\Delta_j^{(b)} = -\Delta_j + \delta_j$, where $\delta_j \in [-\delta/2, \delta/2]$ is a random variable characterizing symmetry-breaking perturbations (see details in Sec. VI of SM [65]). Figure 2(c) plots the averaged IPR and mcom as a function of δ, showing that the NHSE persists even with deviations up to 25% ($\delta = 3$) from perfectly antisymmetric disorder configuration. This demonstrates the robustness of reemergent NHSE against imperfect antisymmetric disorder, extending its applicability beyond fine-tuned scenarios.

Phase diagram—In order to determine the phase diagrams of the Anderson localization to delocalization transitions with the emergence of skin modes, due to the triple interplay of antisymmetric disorder, nonreciprocal hopping and interchain coupling, we calculate the winding number and mcom for different parameters. The winding number in real space is defined as [51]

$$w(E_b) = \frac{1}{N'} \mathrm{Tr}'(\hat{Q}^{\dagger}[\hat{Q}, \hat{X}]), \tag{5}$$

where $\hat{Q}$ is a positive-definite Hermitian matrix, which is obtained by the polar decomposition $(\hat{\mathcal{H}} - E_b) = \hat{Q}\,\hat{P}$,

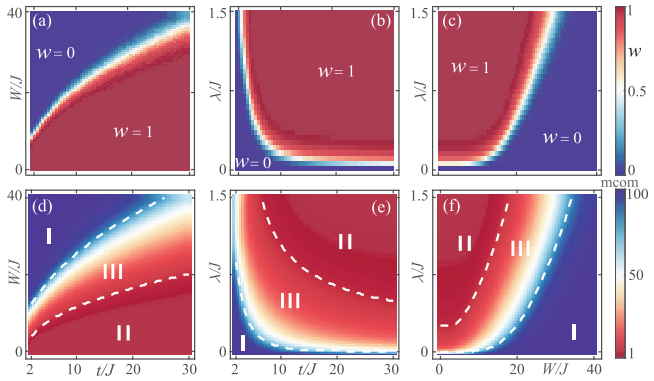

FIG. 3. (a)–(c) Winding number w and (d)–(f) mcom, under antisymmetric disorder, in the (W, t) plane with $\lambda/J = 1$ [(a),(d)], the (λ, t) plane with $W/J = 12$ [(b),(e)], and the (λ, W) plane with $t/J = 14$ [(c),(f)]. Regions I, II, and III correspond to Anderson localization, skin-mode localization, and a mixture of the two, respectively. The results are averaged over 1200 disorder realizations with $\gamma/J = 1$ and $N = 200$.

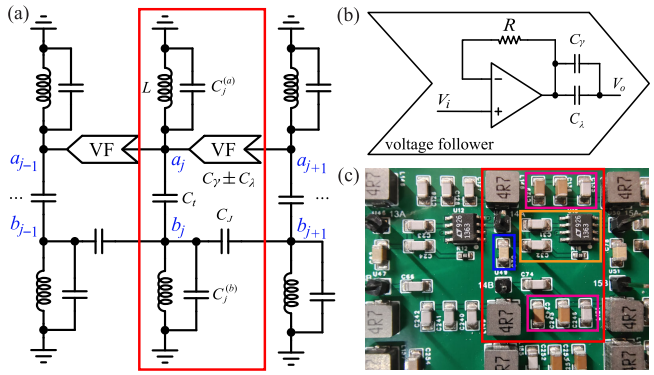

FIG. 4. (a) Circuit implementation of the coupled HN-Hermitian lattice subject to the correlated disorder, corresponding to the model in Fig. 1(a). The red solid line outlines a unit cell in the circuit lattice. For the HN chain $\{a_j\}$, the nonreciprocal intrachain hopping, represented by capacitors $C_\gamma \pm C_\lambda$, is realized via a voltage follower (VF) with its circuit diagram shown in (b), where the resistor $R = 1$ kΩ is used to ensure its stability. The capacitor C_J denotes the intrachain hopping in the Hermitian chain $\{b_j\}$, C_t represents the interchain hopping. $C_j^{(a)}$ and $C_j^{(b)}$ are disordered capacitances to simulate the correlated disorder. The inductor L is used to adjust the resonance frequency of the circuit. (c) Photograph of the fabricated electric circuit in the enlarged view of a unit cell outlined by the red solid line. The modules outlined by blue, yellow, and pink solid lines denote the capacitor C_t, VF, and capacitor C_J, respectively.

with unitary matrix $\hat{P}$. $\hat{Q}$ and $\hat{P}$ are related to the singular value decomposition $(\hat{\mathcal{H}} - E_b) = \hat{M}\hat{S}\hat{N}^\dagger$, with $\hat{Q} = \hat{M}\hat{N}^\dagger$ and $\hat{P} = \hat{N}\hat{S}\hat{N}^\dagger$. $\hat{X}$ is the coordinate operator, with $X_{jj',ss'} = j\delta_{j,j'}\delta_{s,s'}(s = a, b)$, and Tr' denotes the trace over the middle interval with length N', where the whole chain is cut off from both ends. This definition of the winding number avoids the effects from the system's boundary.

The phase diagrams in the presence of antisymmetric disorder are shown in Figs. 3(a)–3(c), where the phase boundary between the absence $(w = 0)$ and presence $(w = 1)$ of skin modes is clearly visible. We find that, regardless of the disorder strength W, skin modes reappear once the interchain coupling t becomes sufficiently large [see Fig. 3(a)]. Moreover, the phase boundary strongly depends on the asymmetric hopping strength λ [see Figs. 3(b) and 3(c)]. The dependence of the phase diagrams on γ is discussed in Sec. VII of SM [65].

The winding number cannot identify the coexistence regions of skin-mode localization and Anderson localization (see details in Sec. VIII of SM [65]), whereas this distinction can be made using the mcom, as shown in Figs. 3(d)–3(f). Regions I, II, and III correspond to Anderson localization, skin-mode localization, and a mixture of the two, respectively. Moreover, the phase boundary (white dotted line across region I) between the absence and presence of skin modes, determined by mcom, agrees with that obtained from the real-space winding number.

Experimental implementation—We implement electrical circuits to realize Anderson delocalization with reemergent NHSE in coupled HN-Hermitian chains induced by correlated disorder. Figure 4(a) shows the designed circuit network, where the unit cell containing sublattices a_j and b_j is outlined by the red solid line. In the HN chain a_j, the nonreciprocal hopping between nodes j and $j + 1$, represented by capacitors $C_\gamma \pm C_\lambda$, is implemented using a voltage follower [36] [see its circuit in Fig. 4(b)]. In the Hermitian chain b_j, the hopping is realized by capacitor C_J. C_t denotes the interchain coupling. The correlated disorder is introduced through disordered capacitances $C_j^{(a)}$ and $C_j^{(b)}$. Figure 4(c) shows the fabricated circuit board.

The model in Eq. (1) is represented by the Laplacian $J(\omega)$ of the circuit, which is defined as the response of the voltage vector $\mathbf{V}$ to the input current vector $\mathbf{I}$ by $\mathbf{I}(\omega) = J(\omega)\mathbf{V}(\omega)$. As shown in Fig. 4(a), the circuit Laplacian $J(\omega)$ reads (see details in Sec. IX of SM [65])

$$J(\omega) = i\omega\mathcal{H}_c - \left(2i\omega C_J + i\omega C_t + i\omega C_g + \frac{1}{i\omega L}\right)\mathbb{1}, \quad (6)$$

where 1 is the $2N \times 2N$ identity matrix, and the matrix $\mathcal{H}_c$ is shown in Sec. IX of SM [65].

The circuit Laplacian $J(\omega)$ and $\hat{\mathcal{H}}$ in Eq. (1) share the same eigenstates if we set $C_J = J$, $C_t = t$, $C_J + C_\lambda = \gamma + \lambda$, $C_J - C_\lambda = \gamma - \lambda$, and $C_j^{(\alpha)} = -\Delta_j^{(\alpha)}$ $(\alpha = a, b)$. The eigenstates of $J(\omega)$, corresponding to the circuit frequency $\omega = 2\pi f$, can be obtained by measuring the voltage response at the circuit nodes.

Figures 5(a) and 5(b) show the measured site-resolved voltage distributions $|V_{a,j}| + |V_{b,j}|$, subject to the antisymmetric disorder. We resonantly excite the circuit at different

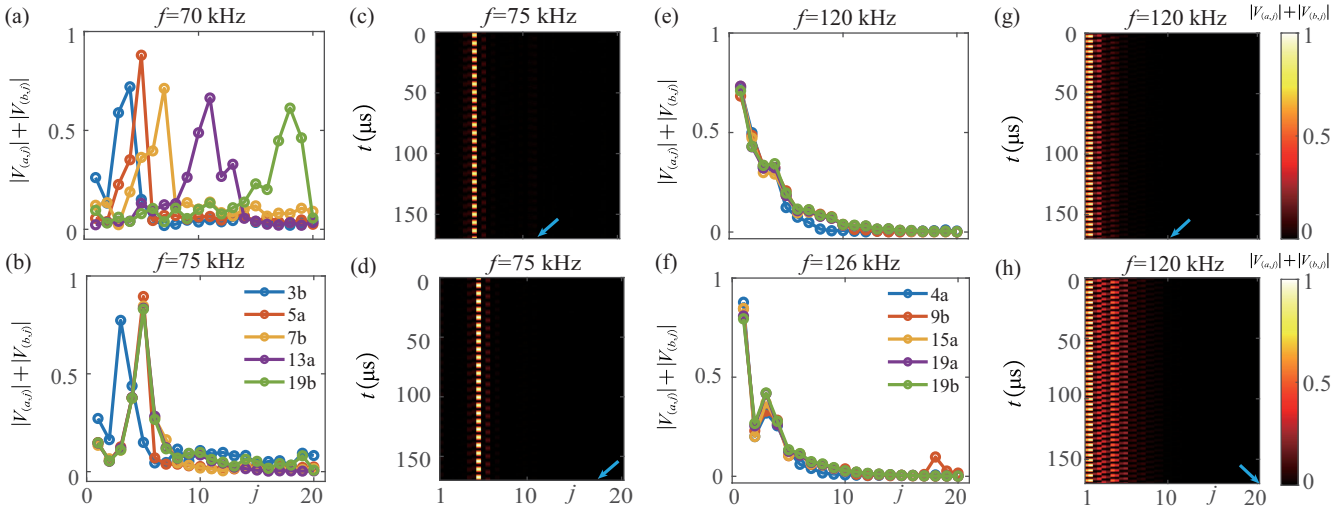

FIG. 5. (a),(b) Measured site-resolved voltage distributions $|V_{a,j}| + |V_{b,j}|$ (j is unit-cell index) at resonance frequencies $f = 70$ kHz (a) and $f = 75$ kHz (b) for weak interchain hopping C_t with $C_\gamma = C_\lambda = C_J = C_t = 100$ nF, $L = 4.7$ μH, and $C_j^{(a)} = -C_j^{(b)} \in [-6C_J, 6C_J]$. The legend "$j\alpha$" ($\alpha = a, b$) in (b) indicates the excitation at the jth site of the chain α. (c),(d) Measured temporal voltage responses excited at the 11th (c) and 17th (d) unit cells, indicated by the blue arrows, for the weak interchain hopping with $f = 75$ kHz. (e),(f) Measured voltage distributions and (g),(h) temporal voltage responses for the strong interchain hopping C_t with $C_\gamma = C_\lambda = C_J = 47$ nF, $C_t = 1$ μF, $L = 4.7$ μH, and $C_j^{(a)} = -C_j^{(b)} \in [-6C_J, 6C_J]$.

nodes with resonance frequencies $f = 70$ kHz and $f = 75$ kHz, respectively, and then measure the voltages at all the nodes. For weak interchain hopping strength C_t, we observe the Anderson-localized voltages distributions [see Figs. 5(a) and 5(b)]. This localization is further confirmed by temporal voltage measurements excited at the 11th and 17th unit cells at $f = 75$ kHz [see Figs. 5(c) and 5(b)], where the voltages remain localized over time, consistent with the steady-state distributions in Figs. 5(a) and 5(b).

We increase the capacitance C_t to enhance the interchain coupling and excite the circuit at frequencies $f = 120$ kHz and $f = 126$ kHz, respectively. The measured site-resolved voltage distributions $|V_{a,j}| + |V_{b,j}|$ [see Figs. 5(e) and 5(f)], excited at different nodes under antisymmetric disorder, reveal reemergent skin effects, consistent with theoretical predictions. In contrast, voltages remain localized under symmetrically correlated disorder (see details in Sec. X of SM [65]). Temporal voltage measurements [see Figs. 5(g) and 5(h)], excited at the 11th and 20th unit cells at frequency $f = 120$ kHz, show voltage propagation along the left boundary, confirming the Anderson delocalization with the reemergent NHSE. These results experimentally demonstrate the antisymmetrical disorder-induced reemergent NHSE in a nonreciprocal chain coupled to a Hermitian chain. Our circuit simulations further confirm the robustness of reemergent NHSE against imperfections in the antisymmetric disorder, which are inevitable in practical systems, thereby extending its applicability beyond fine-tuned conditions.

Conclusion—In summary, we have shown that coupled HN and Hermitian chains with antisymmetrically correlated disorder exhibit a topological Anderson localization-delocalization transition and a robust NHSE, phenomena absent in Hermitian systems. While an isolated disordered HN chain remains localized, coupling to a disordered Hermitian chain with antisymmetric disorder induces an Anderson delocalization. Notably, strong interchain coupling universally leads to Anderson delocalization, accompanied by the reemergent NHSE, regardless of the disorder strength. The topological character of this transition is captured by a real-space winding number. Our electrical-circuit realization reproduces these effects in site-resolved voltage measurements, in excellent agreement with theoretical predictions.

Furthermore, our theoretical and experimental results demonstrate that Anderson delocalization with reemergent NHSE remains robust even in the presence of imperfect antisymmetric disorder. This indicates that correlated disorder can drive Anderson delocalization and stabilize the NHSE in strongly disordered systems, extending beyond finely tuned conditions. This proof of concept highlights that, when combined with interchain coupling, correlated disorder serves as a tunable control parameter to induce transitions between localized and delocalized phases and to reestablish the NHSE. This tunability opens avenues for applications in quantum switches and devices, where wave transport properties can be dynamically modulated via interchain coupling. Looking ahead, it will be compelling to extend this framework to higher-dimensional disordered non-Hermitian systems, where symmetry may play a crucial role in shaping Anderson transitions. Additionally, incorporating interactions could reveal new insights into the interplay of correlated disorder, non-Hermiticity, and many-body effects in governing localization and non-Hermitian phenomena.

Acknowledgments—T. L. gratefully acknowledges helpful discussions with Zhongbo Yan. T. L. conceived and initiated the study and acknowledges the support from the National Natural Science Foundation of China (Grant No. 12274142), the Fundamental Research Funds for the Central Universities (Grant No. 2023ZYGXZR020), Introduced Innovative Team Project of Guangdong Pearl River Talents Program (Grant No. 2021ZT09Z109), and the Startup Grant of South China University of Technology (Grant No. 20210012). Y. R. Z. acknowledges the support from the National Natural Science Foundation of China (Grant No. 12475017) and Natural Science Foundation of Guangdong Province (Grant No. 2024A1515010398). W. J. acknowledges the support from the National Natural Science Foundation of China (No. U21A2093) and Introduced Innovative Team Project of Guangdong Pearl River Talents Program (Grant No. 2021ZT09Z109). F. N. is supported in part by the Japan Science and Technology Agency (JST) [via the CREST Quantum Frontiers program Grant No. JPMJCR24I2, the Quantum Leap Flagship Program (Q-LEAP), and the Moonshot R&D Grant No. JPMJMS2061].

Data availability—The data that support the findings of this article are openly available [68].

[1] D. Leykam, K. Y. Bliokh, C. Huang, Y. D. Chong, and F. Nori, Edge modes, degeneracies, and topological numbers in non-Hermitian systems, Phys. Rev. Lett. **118**, 040401 (2017).
[2] R. El-Ganainy, K. G. Makris, M. Khajavikhan, Z. H. Musslimani, S. Rotter, and D. N. Christodoulides, Non-Hermitian physics and PT symmetry, Nat. Phys. **14**, 11 (2018).
[3] S. Yao and Z. Wang, Edge states and topological invariants of non-Hermitian systems, Phys. Rev. Lett. **121**, 086803 (2018).
[4] K. Yokomizo and S. Murakami, Non-Bloch band theory of non-Hermitian systems, Phys. Rev. Lett. **123**, 066404 (2019).
[5] T. Liu, Y.-R. Zhang, Q. Ai, Z. Gong, K. Kawabata, M. Ueda, and F. Nori, Second-order topological phases in non-Hermitian systems, Phys. Rev. Lett. **122**, 076801 (2019).
[6] K. Zhang, Z. Yang, and C. Fang, Correspondence between winding numbers and skin modes in non-Hermitian systems, Phys. Rev. Lett. **125**, 126402 (2020).
[7] N. Okuma, K. Kawabata, K. Shiozaki, and M. Sato, Topological origin of non-Hermitian skin effects, Phys. Rev. Lett. **124**, 086801 (2020).
[8] K. Kawabata, T. Bessho, and M. Sato, Classification of exceptional points and non-Hermitian topological semimetals, Phys. Rev. Lett. **123**, 066405 (2019).
[9] Z. Y. Ge, Y. R. Zhang, T. Liu, S. W. Li, H. Fan, and F. Nori, Topological band theory for non-Hermitian systems from the Dirac equation, Phys. Rev. B **100**, 054105 (2019).
[10] H. Zhao, X. Qiao, T. Wu, B. Midya, S. Longhi, and L. Feng, Non-Hermitian topological light steering, Science **365**, 1163 (2019).
[11] K. Kawabata, K. Shiozaki, M. Ueda, and M. Sato, Symmetry and topology in non-Hermitian physics, Phys. Rev. X **9**, 041015 (2019).
[12] D. S. Borgnia, A. J. Kruchkov, and R.-J. Slager, Non-Hermitian boundary modes and topology, Phys. Rev. Lett. **124**, 056802 (2020).
[13] T. Liu, J. J. He, T. Yoshida, Z.-L. Xiang, and F. Nori, Non-Hermitian topological Mott insulators in one-dimensional fermionic superlattices, Phys. Rev. B **102**, 235151 (2020).
[14] T. Liu, J. J. He, Z. Yang, and F. Nori, Higher-order Weyl-exceptional-ring semimetals, Phys. Rev. Lett. **127**, 196801 (2021).
[15] S. Mu, L. Zhou, L. Li, and J. Gong, Non-Hermitian pseudo mobility edge in a coupled chain system, Phys. Rev. B **105**, 205402 (2022).
[16] K. Li and Y. Xu, Non-Hermitian absorption spectroscopy, Phys. Rev. Lett. **129**, 093001 (2022).
[17] Z. Ren, D. Liu, E. Zhao, C. He, K. K. Pak, J. Li, and G.-B. Jo, Chiral control of quantum states in non-Hermitian spin–orbit-coupled fermions, Nat. Phys. **18**, 385 (2022).
[18] Z.-F. Cai, T. Liu, and Z. Yang, Non-Hermitian skin effect in periodically driven dissipative ultracold atoms, Phys. Rev. A **109**, 063329 (2024).
[19] L. Li, W. X. Teo, S. Mu, and J. Gong, Direction reversal of non-Hermitian skin effect via coherent coupling, Phys. Rev. B **106**, 085427 (2022).
[20] Y. Li, Z.-F. Cai, T. Liu, and F. Nori, Dissipation and interaction-controlled non-Hermitian skin effects, arXiv:2408.12451.
[21] K. Kawabata, T. Numasawa, and S. Ryu, Entanglement phase transition induced by the non-Hermitian skin effect, Phys. Rev. X **13**, 021007 (2023).
[22] W.-Z. Ling, Z.-F. Cai, and T. Liu, Interaction-induced second-order skin effect, Phys. Rev. B **111**, 205418 (2025).
[23] Z.-F. Cai, X. Wang, Z.-X. Liang, T. Liu, and F. Nori, Chiral-extended photon-emitter dressed states in non-Hermitian topological baths, Phys. Rev. A **111**, L061701 (2025).
[24] Z.-F. Cai, Y.-C. Wang, Y.-R. Zhang, T. Liu, and F. Nori, Versatile control of nonlinear topological states in non-Hermitian systems, arXiv:2411.10398.
[25] A. Regensburger, C. Bersch, M. A. Miri, G. Onishchukov, D. N. Christodoulides, and U. Peschel, Parity–time synthetic photonic lattices, Nature (London) **488**, 167 (2012).
[26] H. Jing, S. K. Özdemir, X. Y. Lü, J. Zhang, L. Yang, and F. Nori, $\mathcal{PT}$-symmetric phonon laser, Phys. Rev. Lett. **113**, 053604 (2014).
[27] H. Hodaei, M. A. Miri, M. Heinrich, D. N. Christodoulides, and M. Khajavikhan, Parity-time–symmetric microring lasers, Science **346**, 975 (2014).
[28] B. Peng, Ş. K. Özdemir, F. Lei, F. Monifi, M. Gianfreda, G. L. Long, S. Fan, F. Nori, C. M. Bender, and L. Yang, Parity–time-symmetric whispering-gallery microcavities, Nat. Phys. **10**, 394 (2014).
[29] B. Peng, Ş. K. Özdemir, S. Rotter, H. Yilmaz, M. Liertzer, F. Monifi, C. M. Bender, F. Nori, and L. Yang, Loss-induced suppression and revival of lasing, Science **346**, 328 (2014).

[30] C. Leefmans, A. Dutt, J. Williams, L. Yuan, M. Parto, F. Nori, S. Fan, and A. Marandi, Topological dissipation in a time-multiplexed photonic resonator network, Nat. Phys. **18**, 442 (2022).
[31] M. Parto, C. Leefmans, J. Williams, F. Nori, and A. Marandi, Non-Abelian effects in dissipative photonic topological lattices, Nat. Commun. **14**, 1440 (2023).
[32] C. R. Leefmans, M. Parto, J. Williams, A. Dutt G. H. Y. Li, F. Nori, and A. Marandi, Topological temporally mode-locked laser, Nat. Phys. **20**, 852 (2024).
[33] J. Zhang, B. Peng, Ş. K. Özdemir, K. Pichler, D. O. Krimer, G. Zhao, F. Nori, Y. X. Liu, S. Rotter, and L. Yang, A phonon laser operating at an exceptional point, Nat. Photonics **12**, 479 (2018).
[34] Y. Choi, C. Hahn, J. W. Yoon, and S. H. Song, Observation of an anti-PT-symmetric exceptional point and energy-difference conserving dynamics in electrical circuit resonators, Nat. Commun. **9**, 2182 (2018).
[35] T. Helbig, T. Hofmann, S. Imhof, M. Abdelghany, T. Kiessling, L. W. Molenkamp, C. H. Lee, A. Szameit, M. Greiter, and R. Thomale, Generalized bulk–boundary correspondence in non-Hermitian topolectrical circuits, Nat. Phys. **16**, 747 (2020).
[36] J. Wu, Z. Wang, Y. Biao, F. Fei, S. Zhang, Z. Yin, Y. Hu, Z. Song, T. Wu, F. Song, and R. Yu, Non-Abelian gauge fields in circuit systems, Nat. Electron. **5**, 635 (2022).
[37] D. Zou, T. Chen, W. He, J. Bao, C. H. Lee, H. Sun, and X. Zhang, Observation of hybrid higher-order skin-topological effect in non-Hermitian topolectrical circuits, Nat. Commun. **12**, 7201 (2021).
[38] J. Hu, R.-Y. Zhang, Y. Wang, X. Ouyang, Y. Zhu, H. Jia, and C. T. Chan, Non-Hermitian swallowtail catastrophe revealing transitions among diverse topological singularities, Nat. Phys. **19**, 1098 (2023).
[39] X. Zhang, C. Wu, M. Yan, and G. Chen, Observation of non-Hermitian pseudo-mobility-edge in a coupled electric circuit ladder, Phys. Rev. B **111**, 014304 (2025).
[40] K. Yamamoto, M. Nakagawa, K. Adachi, K. Takasan, M. Ueda, and N. Kawakami, Theory of non-Hermitian fermionic superfluidity with a complex-valued interaction, Phys. Rev. Lett. **123**, 123601 (2019).
[41] M. Nakagawa, N. Tsuji, N. Kawakami, and M. Ueda, Dynamical sign reversal of magnetic correlations in dissipative Hubbard models, Phys. Rev. Lett. **124**, 147203 (2020).
[42] N. Hatano and D. R. Nelson, Localization transitions in non-Hermitian quantum mechanics, Phys. Rev. Lett. **77**, 570 (1996).
[43] N. Hatano and D. R. Nelson, Non-Hermitian delocalization and eigenfunctions, Phys. Rev. B **58**, 8384 (1998).
[44] J. Feinberg and A. Zee, Non-Hermitian localization and delocalization, Phys. Rev. E **59**, 6433 (1999).
[45] Z. Gong, Y. Ashida, K. Kawabata, K. Takasan, S. Higashikawa, and M. Ueda, Topological phases of non-Hermitian systems, Phys. Rev. X **8**, 031079 (2018).
[46] K. Kawabata and S. Ryu, Nonunitary scaling theory of non-Hermitian localization, Phys. Rev. Lett. **126**, 166801 (2021).
[47] H. Jiang, L.-J. Lang, C. Yang, S.-L. Zhu, and S. Chen, Interplay of non-Hermitian skin effects and Anderson localization in nonreciprocal quasiperiodic lattices, Phys. Rev. B **100**, 054301 (2019).
[48] C. Wang and X. R. Wang, Level statistics of extended states in random non-Hermitian Hamiltonians, Phys. Rev. B **101**, 165114 (2020).
[49] S. Longhi, Topological phase transition in non-Hermitian quasicrystals, Phys. Rev. Lett. **122**, 237601 (2019).
[50] A. F. Tzortzakakis, K. G. Makris, and E. N. Economou, Non-Hermitian disorder in two-dimensional optical lattices, Phys. Rev. B **101**, 014202 (2020).
[51] J. Claes and Taylor L. Hughes, Skin effect and winding number in disordered non-Hermitian systems, Phys. Rev. B **103**, L140201 (2021).
[52] X. Luo, T. Ohtsuki, and R. Shindou, Universality classes of the Anderson transitions driven by non-Hermitian disorder, Phys. Rev. Lett. **126**, 090402 (2021).
[53] C. C. Wanjura, M. Brunelli, and A. Nunnenkamp, Correspondence between non-Hermitian topology and directional amplification in the presence of disorder, Phys. Rev. Lett. **127**, 213601 (2021).
[54] S. Weidemann, M. Kremer, S. Longhi, and A.Szameit, Coexistence of dynamical delocalization and spectral localization through stochastic dissipation, Nat. Photonics **15**, 576 (2021).
[55] Q. Lin, T. Li, L. Xiao, K. Wang, W. Yi, and P. Xue, Observation of non-Hermitian topological Anderson insulator in quantum dynamics, Nat. Commun. **13**, 3229 (2022).
[56] H. Liu, M. Lu, Z.-Q. Zhang, and H. Jiang, Modified generalized Brillouin zone theory with on-site disorder, Phys. Rev. B **107**, 144204 (2023).
[57] E. Abrahams, P. W. Anderson, D. C. Licciardello, and T. V. Ramakrishnan, Scaling theory of localization: Absence of quantum diffusion in two dimensions, Phys. Rev. Lett. **42**, 673 (1979).
[58] P. W. Brouwer, C. Mudry, B. D. Simons, and A. Altland, Delocalization in coupled one-dimensional chains, Phys. Rev. Lett. **81**, 862 (1998).
[59] H. C. F. Martens, Delocalization in weakly coupled disordered wires: Application to conjugated polymers, Phys. Rev. Lett. **96**, 076603 (2006).
[60] D. Weinmann and S. N. Evangelou, Parity-dependent localization in n strongly coupled chains, Phys. Rev. B **90**, 155411 (2014).
[61] P. Bordia, H. P. Lüschen, S. S. Hodgman, M. Schreiber, I. Bloch, and U. Schneider, Coupling identical one-dimensional many-body localized systems, Phys. Rev. Lett. **116**, 140401 (2016).
[62] T. Iadecola and M. Žnidarič, Exact localized and ballistic eigenstates in disordered chaotic spin ladders and the Fermi-Hubbard model, Phys. Rev. Lett. **123**, 036403 (2019).
[63] X. Lin and M. Gong, Fate of localization in a coupled free chain and a disordered chain, Phys. Rev. A **109**, 033310 (2024).
[64] X. Lin, M. Gong, and G.-C. Guo, From single-particle to many-body mobility edges and the fate of overlapped spectra in coupled disorder models, arXiv:2307.01638.
[65] See Supplemental Material at http://link.aps.org/supplemental/10.1103/lpm2-vcb4 for (i) physical mechanism, (ii) eigenenergy-resolved IPR and mcom, (iii) finite-size effects, (iv) biorthogonal inverse participation ratio, (v) quenched dynamics, (vi) robustness of Anderson delocalization against imperfect antisymmetric disorder,

(vii) dependence of phase diagrams on γ, (viii) coexistence region of Anderson and skin-mode localization, (ix) circuit implementation of the model, and (x) experimental results of HN-Hermitian coupled chains subject to the symmetric disorder, which includes Ref. [66].

[66] Y.-X. Xiao and C. T. Chan, Topology in non-Hermitian Chern insulators with skin effect, Phys. Rev. B **105**, 075128 (2022).

[67] P. Molignini, O. Arandes, and E. J. Bergholtz, Anomalous skin effects in disordered systems with a single non-Hermitian impurity, Phys. Rev. Res. **5**, 033058 (2023).

[68] W. W. Jin, W. Ju, and T. Liu, Supporting Experimental Data for Manuscript "Anderson Delocalization in Strongly-Coupled Disordered Non-Hermitian Chains," 10.5281/zenodo.16411878.